the higher reversion temperature, but the smaller stabilization effect allows progressive strengthening to proceed throughout the series of transformation cycles studied.

In general, the strengthening of austenitic stainless steels by the reverse martensite transformation appears to be limited by three main factors. Firstly, little deformation of the retained austenite is produced by the direct and reverse martensite transformations and hence, unlike iron–nickel alloys, significant strengthening occurs only in those regions which actually transform. Secondly, only small amounts of martensite are produced in these steels by cooling below the M_S temperature, although in some steels prolonged isothermal holding below M_S can produce substantial amounts of martensite [6]. Finally, the cumulative strengthening action of repeated transformation cycles is restricted by the development of austenite stabilization.

Acknowledgements

This work was carried out with the support of the Science Research Council and of the Procurement Executive, Ministry of Defence. Acknowledgements are also made to Professor J. G. Ball for the provision of research facilities, and to International Nickel Ltd for preparing the alloys.

References

1. G. KRAUSS JUN and M. COHEN, *Trans. Met. Soc. AIME* **224** (1962) 1212.
2. G. KRAUSS JUN, *Acta Met.* **11** (1963) 499.
3. B. HYATT and G. KRAUSS, *Trans. ASM* **61** (1968) 168.
4. C. APPLE and G. KRAUSS, *Met. Trans.* **2** (1971) 1785.
5. T. K. KOPPENAAL, *ibid* **3** (1973) 1549.
6. V. V. SAGARADZE and K. A. MALYSHEV, *Metalloved. Term. Obrab. Met.* **14** (1972) 733.
7. K. A. MALYSHEV and V. V. SAGARADZE, *Phys. Met. Metallog.* **25** (5) (1968) 135.
8. K. A. MALYSHEV, N. A. BORODINA and V. A. MIRMEL'SHTEYN, *Trudy Inst. Fiz. Met.* **20** (1958) 339.
9. J. F. BREEDIS, *Trans. Met. Soc. AIME* **236** (1966) 218.
10. T. H. COLEMAN and D. R. F. WEST, *Metallography* **7** (1974) 203.
11. J. F. BREEDIS, *Trans. Met. Soc. AIME* **230** (1964) 1583.
12. H. SMITH and D. R. F. WEST, *J. Mater. Sci.* **8** (1973) 1413.
13. *Idem, Metals Tech.* **1** (1974) 37.
14. *Idem, ibid* **6** (1974) 295.
15. J. F. BREEDIS and W. D. ROBERTSON, *Acta Met.* **10** (1962) 1077.
16. S. R. THOMAS and G. KRAUSS, *Trans. Met. Soc. AIME* **239** (1967) 1136.

Received 14 February
and accepted 18 March 1975

H. SMITH
Jones and Laughlin Steel Corporation, Pittsburgh, Pennsylvania, USA
D. R. F. WEST
Department of Metallurgy and Materials Science, Imperial College, London, UK

Variation of MC carbide geometry with local solidification time in cast Inconel 713 C alloy

In as-cast polycrystalline nickel-base superalloys, MC-type carbides contribute to high temperature grain-boundary strengthening. In these carbides, M is tantalum, niobium, zirconium, titanium or molybdenum [1-2]. Among them TaC and NbC are very stable, whereas multicomponent carbides are metastable with a tendency towards dissociation or dissolution during long service at high temperature. In the as-cast alloy, no orientation relationship has been established between MC carbide and matrix [3-5].

In unidirectionally solidified monocrystalline or polycrystalline superalloys, the MC carbide morphology has been described as dendritic and unconnected near the chill, with tendencies to form an interconnected, interdendritic network away from the chill [5, 6]. An increase in particle size was observed with distance from the chill [5, 6].

The purpose of the present investigation was to establish quantitatively the dependence of MC carbide geometry on local solidification time [7] in unidirectionally solidified Inconel 713 C alloy.

The alloy was vacuum-melted and solidified in moulds (4.50 cm × 4.50 cm × 15 cm) made of "fiberchrome", an insulating material, with open bottom placed against a water-cooled copper chill [8]. All surfaces of the mould cavity, runner and risers were coated with "zircon" wash. Cooling curves were recorded using Pt/Pt–10% Rh thermocouples inserted horizontally along the height of the ingot at 1, 2, 3

© 1975 Chapman and Hall Ltd.

and 4 cm from the chill. To extend the spectrum of cooling rates, rods of the alloy (10 cm long with diameters of 0.5, 0.65 and 0.80 cm) were cast in a copper mould.

Specimens from various ingots were polished and etched with Marble's reagent to reveal the solidification structure, or electropolished using a 10% perchloric acid solution in methanol at − 30°C and 12 V. Microstructural examination was conducted by: (1) optical microscopy to evaluate carbide shape and size by quantitative metallographic techniques; (2) scanning electron microscopy to study details of the carbide geometry. The specimens used were deeply etched with Marble's reagent for 1 to 2 h to dissolve away the matrix and γ' precipitate.

The volume percent MC carbide was determined by a two dimensional systematic point counting procedure based on a coarse-mesh lattice criterion [9] and also by computerized image analysis (Quantimet 720).

Evaluation of carbide shape and size proved to be very difficult because of the intricate geometry of the particles and the lack of appropriate procedure for making statistically valid measurements. Carbide particle shape was determined using Hausner's procedure for metal powders [10]. The rectangle of smallest area encompassing the particle outline in a plane cross-section was drawn around the particle and the ratio, E, or its short-to-long side ("elongation factor") was calculated. The ratio, B, of the area of the particle cross-section to the area of the rectangle ("bulkiness factor") was also calculated. For each specimen, two bulkiness factors and two elongation factors were calculated, one normal and one weighted. Normal bulkiness and elongation factors attach equal weight to each particle regardless of size, whereas weighted bulkiness and elongation factors attach to each particle a weight which is proportional to its size. Thus:

$$\text{normal } B = \frac{1}{N}\sum_{i=1}^{N}\frac{C_i}{A_i \,.\, B_i},$$

$$\text{normal } E = \frac{1}{N}\sum_{i=1}^{N}\frac{B_i}{A_i}$$

$$\text{weighted } B = \sum_{i=1}^{N}\frac{C_i}{A_i \,.\, B_i}\cdot\frac{C_i}{T},$$

$$\text{weighted } E = \sum_{i=1}^{N}\frac{B_i}{A_i}\cdot\frac{C_i}{T}$$

where A_i is long side of rectangle, B_i is short side of rectangle, C_i is particle cross-sectional area, N is number of particle outlines and T is area of all particle outlines considered.

Application of Dehoff's modification [11] of Saltykov's analysis for evaluating other parameters by quantitative metallography was excluded, because the assumption that particles could be assimilated with prolate or oblate ellipsoids of revolution of constant axial ratio was found in the present case to be unrealistic. The following procedures were, therefore, adopted.

The carbide–matrix interface area per unit volume of matrix, S_v, was calculated from [12]:

$$S_v = \frac{4}{\pi}\bar{L} \tag{1}$$

where $\bar{L}$ is the total length of particle outlines per unit area of transverse section, averaged over several sections.

The number of particle outlines per unit area of transverse section, N, was determined on random sections for each specimen. Finally, the average particle outline size (diameter), d, was determined by linear analysis [12].

The variation of carbide cross-sectional geometry, with cooling rate is illustrated in Fig. 1. Fig. 1a is a photomicrograph of a specimen taken at 0.3 in. from the chill and corresponds to a local solidification time t_f = 140 sec. Fig. 1b is that of a specimen taken at 2.40 in. from the chill and corresponds to t_f = 1500 sec. Fig. 1c is that of a specimen taken from a chill-cast rod, 0.65 cm in diameter and corresponds to t_f = 2 sec. On such plane sections, carbides appeared to be isolated, often exhibiting a script-like morphology. Examination of deeply etched specimens by scanning electron microscopy (Fig. 2) revealed that carbides were interconnected both in unidirectionally solidified specimens and in specimens obtained from chill-cast rods. Branching in dendritic carbides became coarser with increasing local solidification time.

The alloy contained an average vol% MC carbide of about 1.0, which remained practically constant with increasing local solidification time. These results differ from previous findings [4] indicating that in columnar MAR-M200 the

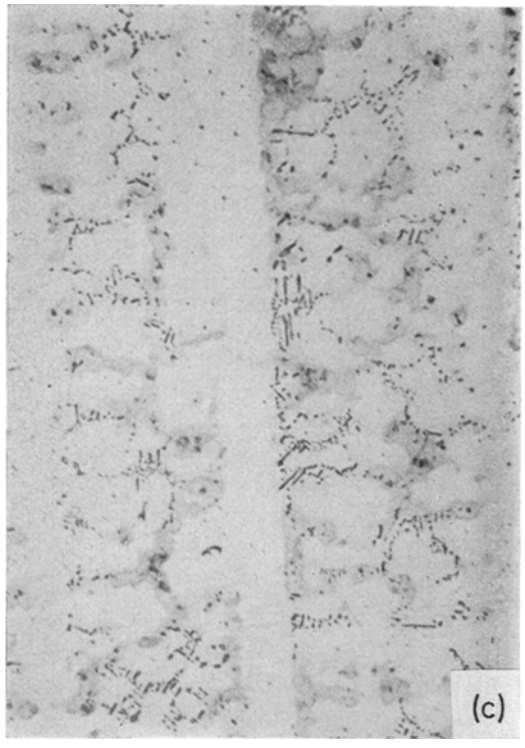

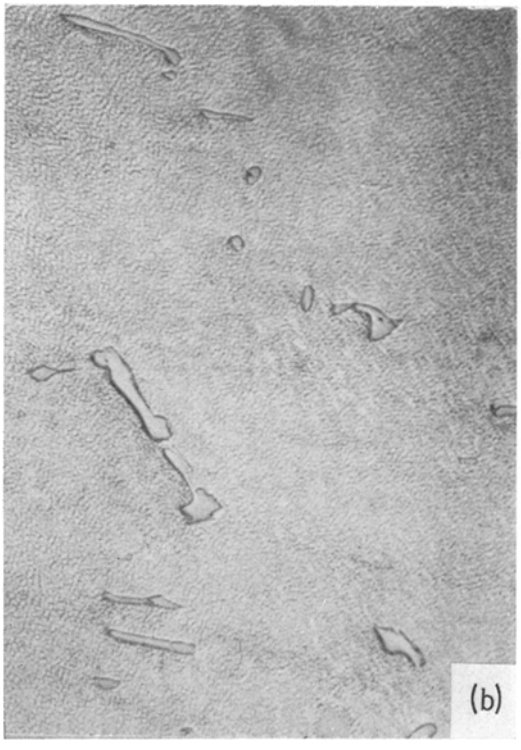

Figure 1 Photomicrographs illustrating the variation of MC carbide geometry with local solidification time in Inconel 713C, × 400. (a), (b) Specimens taken from a unidirectionally solidified ingot at 0.3 in. and 2.40 in. from the chill, respectively; (c) specimen taken from a chill-cast rod.

volume fraction carbide increased from 0.01 near the chill to 0.03 away from it.

Normal and weighted bulkiness and elongation factors did not change appreciably with local solidification time. They were approximately equal to 0.6 and 0.4, respectively, for local solidification times varying between 100 and 1900 sec. For each specimen, however, the weighted bulkiness or elongation factors were lower than the corresponding normal factors. In general, large particles appeared to be more elongated and less bulky than the small ones.

The increase in average particle outline size, $\bar{d}$, with local solidification time, t_f, is illustrated in Fig. 3. The decrease of the number of particle outlines per unit area of cross-section, N, and that of the total carbide-matrix interfacial area per unit volume of matrix, S_v, with increasing local solidification time are illustrated in Figs. 4 and 5, respectively. It has been shown elsewhere

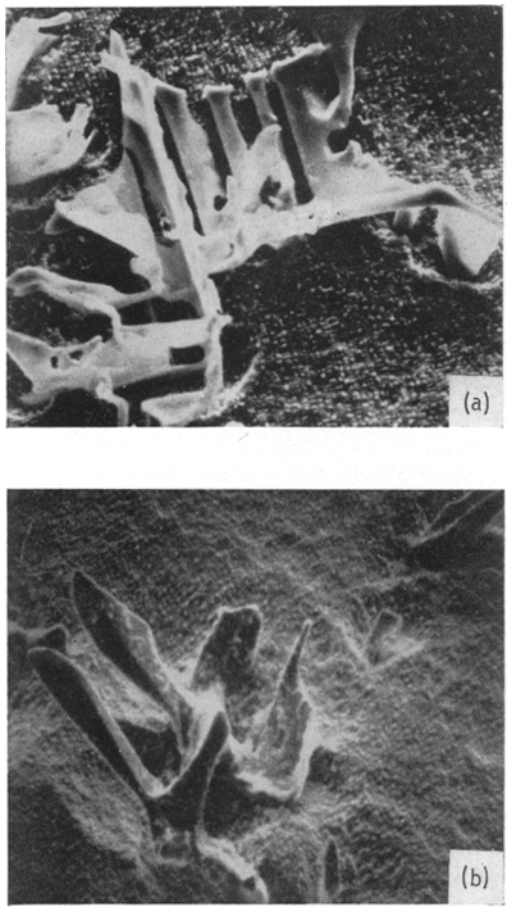

Figure 2 Scanning electron micrographs illustrating the variation of MC carbide geometry with local solidification time in unidirectionally solidified Inconel 713C alloy, × 1500. (a) Specimen taken at 0.3 in. from the chill; (b) specimen taken at 2.40 in. from the chill.

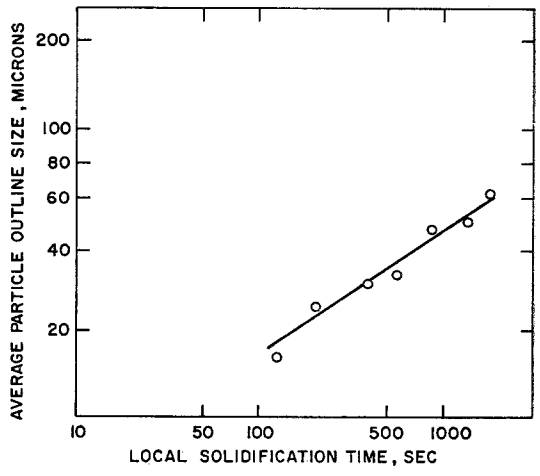

Figure 3 Average particle outline size versus local solidification time. MC carbide in Inconel 713C.

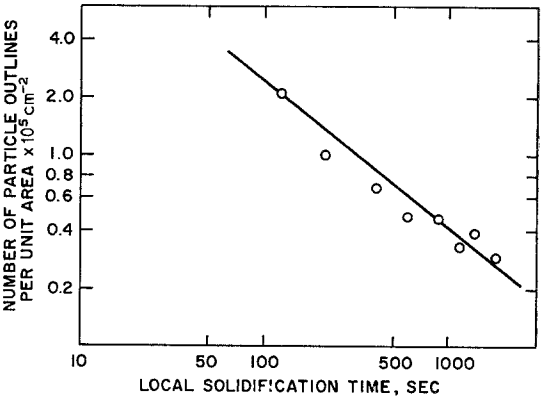

Figure 4 Number of particle outlines per unit area versus local solidification time. MC carbide in Inconel 713C.

[8] that carbides nucleate and grow in the liquid ahead of the solid–liquid interface. Assuming that the rate of nucleation is relatively independent of local solidification time, the curves in Figs. 4 and 5 would then indicate that coarsening of carbide particles surrounded by liquid controls final particle size. In this case coarsening would consist of two components: diffusional coarsening ("ripening") and collisional coalescence. The contribution of ripening may be predicted using the Lifshitz-Wagner equation [13], neglecting growth due to solidification, and assuming that growth is diffusion controlled and that the time during which ripening operates is proportional to the local solidification time. For cases when temperature varies the Lifshitz-Wagner equation can be

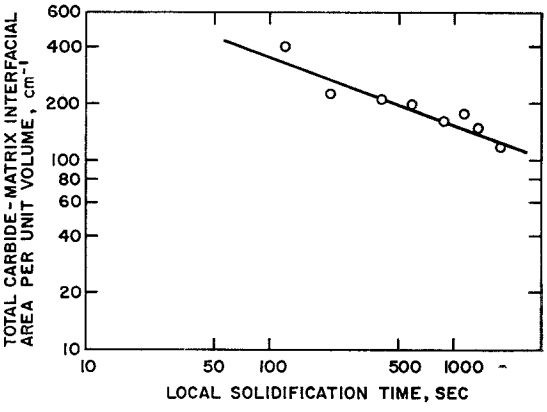

Figure 5 Total carbide-matrix interfacial area per unit volume versus local solidification time. MC carbide in Inconel 713C.

written as:

$$\int_{\bar{d}_0}^{\bar{d}} \mathrm{d}(\bar{d})^3 = \int_0^t k \frac{D}{T} \mathrm{d}t \qquad (2)$$

with

$$k = \frac{64}{9} \frac{\sigma C_0 V_M^2}{\nu R} \qquad (3)$$

where C_0 is equilibrium solubility of carbon in the melt, $\bar{d}$ is the average particle outline size at time t, V_M is the molar volume of carbide based on the formula $(Nb_{0.63}Ti_{0.31}Mo_{0.06})C$ established elsewhere [8], σ is the carbide-liquid interface energy, assumed isotropic, T the absolute temperature at time t, R is the gas constant, ν is the stoichiometric factor (weight fraction of the solute in carbide particles) and D is diffusivity of solute in the liquid, equal to $D_0 e^{-Q/RT}$, where Q is the activation energy for diffusion in the liquid.

Changing the variable from t to T and integrating the left hand side of Equation 2 yields:

$$\bar{d}^3 - \bar{d}_0^3 = k \int_{T_0}^{T_f} \frac{D_0 e^{-Q/RT}}{T} \left(\frac{\mathrm{d}t}{\mathrm{d}T}\right) \mathrm{d}T. \qquad (4)$$

Assuming a parabolic cooling rate:

$$\frac{\mathrm{d}T}{\mathrm{d}t} = -\epsilon_0 \left(\frac{T}{T_0}\right)^2 \qquad (5)$$

and integrating the right hand side yields:

$$\bar{d}^3 - \bar{d}_0^3 = -\frac{kD_0}{\epsilon_0} \left(\frac{RT_0}{Q}\right)^2 \left[\frac{Q}{RT_0} e^{-Q/RT_0} - \frac{Q}{RT_f} e^{-Q/RT_f} + e^{-Q/RT_0} - e^{-Q/RT_f}\right] \qquad (6)$$

where ϵ_0 is intial cooling rate, T_0 is initial temperature and T_f is final temperature, at which solidification is completed.

The following values were adopted for the various parameters in these expressions: $\sigma = 1.2 \times 10^{-5}$ cal cm^{-2} [14], $C_0 = 0.015$ mol cm^{-3} [15], $\nu = 0.132$, $D_0 = 0.1$ cm^2 sec^{-1}, $Q/R = 15\,000$ K, $T_0 = 1561$ K, $T_f = 1501$ K and $V_M = 12.3$ cm^3 mol^{-1}. Combination of the previous equations then yields:

$$\bar{d}^3 - \bar{d}_0^3 = \frac{1.665 \times 10^{-10}}{\epsilon_0}. \qquad (7)$$

Let $\bar{d}_2$ be the average particle outline size measured after completion of solidification at a location at which initial cooling rate is $(\epsilon_0)_2$ and $\bar{d}_1$ that measured at a location at which initial cooling rate is $(\epsilon_0)_1$. It follows that:

$$\bar{d}_2^3 - \bar{d}_1^3 = 1.665 \times 10^{-10} \left[\frac{1}{(\epsilon_0)_2} - \frac{1}{(\epsilon_0)_1}\right]. \qquad (8)$$

At a location 0.3 in. from the chill, $\bar{d}_1 = 16$ μm and $(\epsilon_0)_1 = 0.45$ K sec^{-1}. At another location about 2 in. from the chill, $\bar{d}_2 = 45$ μm and $(\epsilon_0)_2 = 0.07$ K sec^{-1}. In this second case $(\bar{d}_2)_C$, calculated from Equation 8 is about 18.5 μm. The difference between 45 and 18.5 μm would indicate the predominant contribution of collisional coalescence to particle coarsening.

References

1. H. E. COLLINS, *Trans. Amer. Soc. Met.* **62** (1969) 82.
2. J. R. MIHALISIN, G. G. BIEBER and R. T. GRANT, *Trans. Met. Soc. AIME* **242** (1968) 2399.
3. J. F. RADAVICH, Technical Report, Micro-Met Laboratories, Inc, West Lafayette, Indiana.
4. B. J. PIEARCEY, B. H. KEAR and R. W. SMASHEY, *Trans. Amer. Soc. Met.* **60** (1967) 634.
5. B. J. PIEARCEY and R. W. SMASHEY, *Trans. Met. Soc. AIME* **60** (1967) 451.
6. M. GELL and G. R. LEVERANT, *ibid* **242** (1968) 1869.
7. M. C. FLEMINGS, "Solidification Processing" (McGraw-Hill, New York, 1974) p. 22.
8. A. K. BHAMBRI, T. Z. KATTAMIS and J. E. MORRAL, to be published.
9. J. E. HILLIARD and J. W. CAHN, *Trans. Met. Soc. AIME* **221** (1961) 344.
10. H. H. HAUSNER, *Planseeberichte für Pulvermetallurgie* **14** (1966) 75.
11. R. T. DEHOFF, *Trans. Met. Soc. AIME* **224** (1962) 474.
12. R. T. DEHOFF and F. N. RHINES, "Quantitative Microscopy" (McGraw-Hill, New York, 1968).
13. C. WAGNER, *Z. Electrochem.* **65** (1961) 581.
14. T. Z. KATTAMIS, *University of Connecticut, Storrs, Connecticut.*
15. M. HANSEN, "Constitution of Binary Alloys" (McGraw-Hill, New York, 1958).

Received 24 February
and accepted 19 March 1975

S. C. FEGAN
T. Z. KATTAMIS
J. E. MORRAL
Department of Metallurgy,
Institute of Materials Science,
University of Connecticut,
Storrs, Connecticut, USA

A. K. BHAMBRI
Materials Science Research,
Material Aeronautics and Space Administration,
Ames Research Center, California, USA